Microwave current drive for STEP and MAST Upgrade

Simon Freethy[1], *Lorenzo* Figini[2], *Mark* Henderson[1], *Hana* El-Haroun[1], *Bengt* Eliason[4], *Sam* Gibson[1], *Krassimir* Kirov[1], *Alf* Köhn-Seemann[3], *Ivan* Konoplev[1], *Samuli* Saarelma[1], *Ridhima* Sharma[1], *David* Speirs[4], *Roddy* Vann[5], *Helen* Webster[1], *Thomas* Wilson[1] and the STEP team[1]

[1] UKAEA, Culham Science Centre, Abingdon, OX14 3DB, United Kindgom
[2] Istituto per la Scienza e Tecnologia dei Plasmi, Consiglio Nazionale delle Ricerche, 20125 Milano, Italia
[3] University of Stuttgart, IGVP, Pfaffenwaldring 31, 70569 Stuttgart, Germany
[4] University of Strathclyde, 16 Richmond St, Glasgow, G1 1XQ, United Kingdom
[5] University of York, York, YO10 5DD, United Kingdom

Abstract. The UK's Spherical Tokamak for Energy Production (STEP) reactor design program has recently taken the decision to use exclusively microwave-based heating and current drive (HCD) actuators for its reactor concepts. This is based on a detailed assessment considering all viable HCD concepts, covering the grid to plasma efficiency, physics applications, technology maturity, integration, maintenance, and costs. Of the two microwave techniques: Electron Cyclotron (EC) and Electron Bernstein Wave (EBW), EC was deemed the lowest risk and EBW is retained as a potential path to a more efficient, higher performing device. To assess the ECCD efficiency, the GRAY beam tracing code was employed to perform detailed scans of the launcher position, toroidal and poloidal launch angle, and frequency over the first 3 cyclotron harmonics. For EBW, GENRAY/CQL3D were used to estimate the CD efficiency, demonstrating promising results. To reduce the physics uncertainties in present models for EBW coupling and current drive, MAST Upgrade will install two dual frequency (28, 34.8 GHz), 900kW, 5s gyrotrons from Kyoto Fusioneering, as part of the MAST Upgrade enhancements package. This will be accompanied by a flexible 2D steering launcher system to allow midplane co- and counter-CD and above midplane launch for co-direction off-axis CD. Coupling efficiency is quantified by measuring the heating induced by reflected (i.e. non-coupled) power to a plate inserted in the reflected beam path. The experiments will also include EBW driven solenoid-free start-up, increasing power and pulse length by a factor of 10 compared to previous MAST experiments. This presentation will discuss the STEP microwave studies and the MAST Upgrade physics design and capabilities.

1 Introduction

The STEP (Spherical Tokamak for Energy Production) program is the UK's Spherical Tokamak (ST) reactor design endeavour. In the first tranche (2022-2024), the program aims to produce a concept design for a steady state ST reactor, producing ~100 MWe. As such, the auxiliary current drive system is a critical user of recirculating power. Due to the technological advantages of microwave systems, the present STEP concept uses microwave techniques exclusively for the heating and current drive (HCD) system.

Electron Cyclotron Current Drive (ECCD) will be the primary mechanism for current drive due to the relative maturity and flexibility of the technique. Electron Bernstein Wave Current Drive (EBCD) is adopted as the secondary technique, due to the promise of higher overall current drive efficiency and the ability to operate at high density. Due to the relative uncertainty and reduced flexibility of an EBCD system, two plasma concepts are being developed, one which uses ECCD exclusively and one which uses a combination of EBCD and ECCD, where a balance is found which plays to the relative advantages of the two techniques.

For the EC only concept, the ECCD is responsible not only for the steady state plasma in combination with the bootstrap current, but also for the majority of the plasma ramp-up, as space constraints in the spherical tokamak limit the size of the central solenoid. In the EB+EC concept, ECCD is responsible for the ramp-up as the EB coupling scheme requires a critical density and dictates that the launched beam must follow the magnetic field pitch-angle evolution at the O-mode cut-off. This would require a relatively large steering range and is presently considered too technically challenging. For the steady state phase, where overall efficiency is critical, the EBW is responsible for the majority of the current drive, which is predominantly off-axis. Since the EBW has limited radial access in the STEP concepts to $\rho \gtrsim 0.4 - 0.5$, the required central current drive is provided by ECCD.

EBCD is still relatively immature compared to ECCD. To address the uncertainties of EBCD, MAST Upgrade will install two dual frequency gyrotrons (28 and 34.8 GHz), capable of 900 kW (3s) and 800kW (4.5s). The experiment will measure the EBCD efficiency for the first time on an ST and will provide a facility for testing linear coupling, the effect of density perturbations, non-linear coupling effects as well as solenoid-free EBW start-up experiments. This is paired with a theory and modelling effort for STEP and MAST-Upgrade to develop the physics basis for the use of EBCD on a reactor. Here we describe the system design and the analysis which has set the requirements.

2 ECCD optimisation on STEP

As a design principle, we want to minimise the steering required from the ECCD and EBCD launchers. This fact, combined with the fact that microwaves will provide all the auxiliary current through the plasma ramp-up and steady state phases, will in practice mean

that a wider range of frequencies will be required on STEP than for a device like ITER in order to reproduce the desired current profile and provide current profile tailoring.

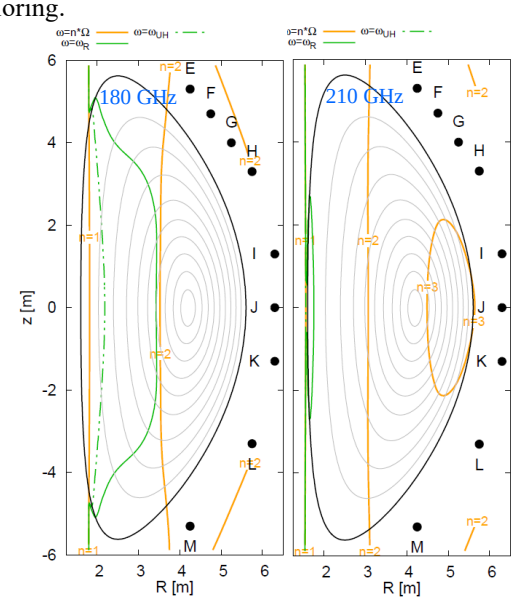

Fig. 1: The plasma equilibrium and candidate launch locations for the SPR-045 concept. Harmonics, X-mode cut-off and upper hybrid resonance are shown for 180 GHz (left) and 210 GHz (right)

To optimise the EC configuration for current drive efficiency, a number of candidate launcher positions were selected, as can be seen in Fig. 1. GRAY [1] was then used in single ray configuration to scan the frequency over fundamental, 2nd and 3rd harmonics (70 – 240 GHz), and toroidal and poloidal angles from each launcher for X and O mode. The result was a rich dataset for the operational space of the ECCD system for that plasma concept [2]. From there, the most efficient configurations were used to fit to the plasma auxiliary current density profile. If the ECCD power assumed by the JETTO simulation is too far from the power required to fit the profile, then another iteration is made.

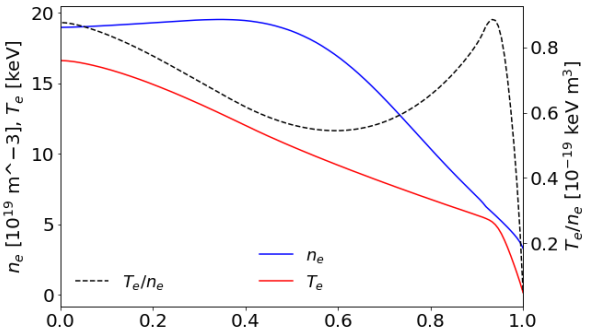

Fig. 2: The electron temperature and density profiles for the SPR-045 plasma concept

Fig. 2 shows the density and temperature profiles for SPR-045, the latest ECCD only plasma concept, and Fig. 1 shows the plasma equilibrium and characteristic frequencies for 180 and 210 GHz for this scenario, along with the labelled candidate launcher positions.

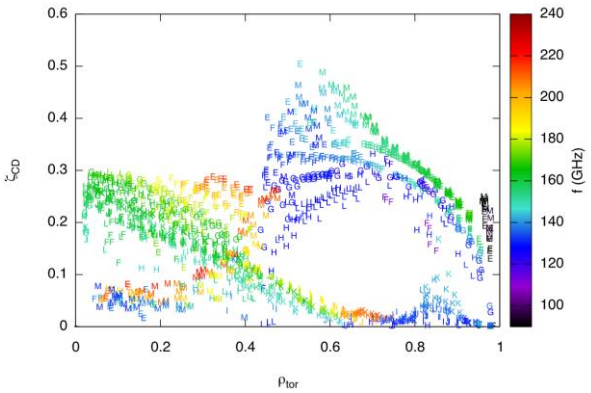

Fig. 3: A selection of the configurations and their normalised current drive efficiency. Launch points are represented by letters and the colour denotes the launch frequency

Fig. 3 shows the current drive efficiency at the radial location of the peak of the current density profile. The values are normalised to [3]

$$\zeta = 3.21 \frac{R_m n_{19}}{T_{keV}} \frac{I}{P} \quad (1)$$

This normalisation is useful for comparing the relative efficiency of ECCD and EBCD in different scenarios. The efficiency ζ is comparable to the optimal values found for DEMO [4], and the most efficient launchers over a wide range of radii are E, F, G and M. For more details of the approach and the resulting shape of this curve, please see [2].

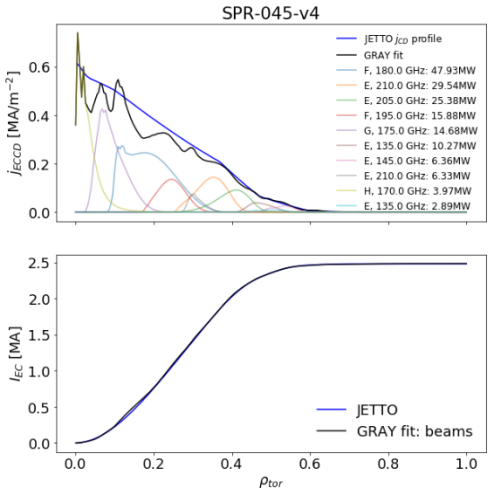

Fig. 4: (a) The current density profile from integrated modelling (JETTO) and GRAY fit to that profile. (b) The cumulative integral of the current density for GRAY and JETTO

The current density and cumulative current profiles were fit to the required auxiliary current and current density profiles using a non-negative least squares (nnls) algorithm and the result for this for SPR-045 is shown in Fig. 4. This leads to a realistic estimate for the total EC power required, as well as the power required in each configuration. Configurations requiring more than 1MW in power are listed in the plot legend of Fig. 4. In total in this scenario, 166 MW is required to drive 2.5 MA of auxiliary current, for a total plasma current of 20.5 MA. The bootstrap fraction is calculated self-

consistently within JETTO with the assumptions for density and thermal transport. However, since for the ST the transport is not well understood and there is limited empirical data, changes in these assumption could lead to large variations in the recirculating power. The exposure of the design to this risk is less for a more efficiecnt current drive methodology, hence the need to develop EBCD.

Modellling for the plasma ramp-up is not yet complete and will be presented at a later date. However, the ramp-up will take place at much lower density than the steady state phase, resulting in higher real terms efficiency from the ECCD system. Then follows a transition from EC dominated current drive to bootstrap dominated current drive at higher density.

3 EBCD on STEP

The STEP EBW concept is still under development, so here we present the analysis approach and some preliminary results of this analysis. A low-field side (LFS) coupling to the EBW via the O-X-B process was chosen, as coupling from the high-field side (HFS), such as was demonstrated in [5], is limited in density by the left-hand X-mode cut-off, presenting too strict a density limitation, and the beam must pass through the fundamental harmonic in order to reach the upper hybrid resonance, where the conversion to EBW occurs. For the plasma parameters envisaged for the STEP flat-top, a high percentage of this power would be absorbed at the fundamental harmonic, making this impractical. Direct X-B tunnelling from the LFS is also not appropriate as the overall coupling efficiency is very sensitive to the density gradient and is only efficient at $k_0 L_n$ values far below what is expected for any of the STEP concepts.

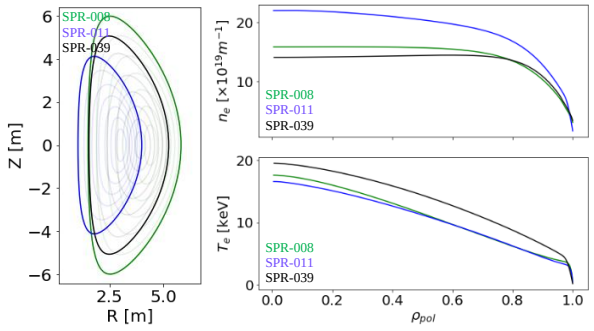

Fig. 5: Equilibria, density, and temperature profiles for SPR-008, SPR-011 and SPR-039

Initially we're interested in what the expected current drive efficiency would be for perfect coupling, over what radial range we can expect to drive current, and then whether or not the linear coupling scheme looks feasible for the STEP concepts. More advanced analysis which looks into the potential impact of non-linear effects and density perturbations will be examined later in combination with the MAST Upgrade EBW system.

3.1 Penetration and current drive efficiency

For the assessment of current drive efficiency of EBCD in these scenarios, GENRAY [6] was used for the ray-tracing component and CQL3D [7] for the radiative transport and current drive calculations. For each of the concepts, the EBWs are launched between the fundamental and second harmonics as normally access at higher harmonics is not possible as the presence of an O-mode cut-off is required. The launch angles are restricted to the critical angles required for coupling and the height and frequency are scanned over the relevant ranges. Several concepts were analysed and Fig. 5 shows equilibria, density, temperature profiles for three of these. For more a more detailed account of the study, see [8].

Exceptional current drive efficiencies were found, as shown in Fig. 6, with normalised efficiencies up to 1.5, three times higher than the ECCD in a similar region. This makes EBCD a very promising avenue and would significantly lower the re-circulating power requirements for the reactor.

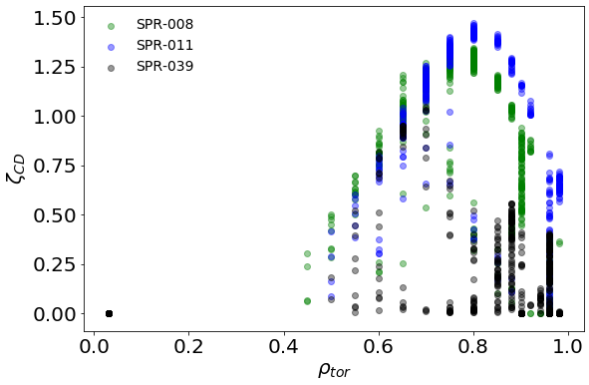

Fig. 6: normalised current drive efficiencies for the three different plasma concepts

Access to radii less than $\rho_{tor} \simeq 0.5$ is limited primarily by a combination of Doppler broadening of the resonance and the non-monotonic B-field profile typical of the high-β ST reactor [8]. The radial restriction was approximately the same across the ST concepts we examined. The limited radial range for EBW means that ECCD is required for core current drive to avoid the formation of a current hole in the plasma centre, which could give rise to MHD instabilities. This in turn sets a limitation on both the lowest and highest operating densities. True high-density operation, without ECCD, can only be reasonably achieved by increasing the EBW penetration and this can be done by operating at lower temperature. In principle, a lower temperature, higher density operating point would be preferable, but it remains to be seen if such a scenario can be self-consistently achieved.

3.2 Coupling estimates

The EBWs are coupled to from the low field side of the plasma via the O-X-B scheme [9]–[11]. For a plane wave approaching a plasma slab at the critical angle, this conversion is 100%, for increasing deviations from the

critical angle, a tunnelling effect determines the rate at which the coupling efficiency falls off. We can estimate this from an analytical formula developed by Mjølhus [12], in combination with ray-tracing. This effect determines not only the steering angle sensitivity, but also the acceptable divergence of a gaussian beam, where finite divergence takes power away from the critical wavevectors into less efficient ones. The beam divergence effect can be quantified by the following [13]:

$$< \tau_{OX} > \simeq \left(1 + 3\frac{\kappa}{z_R} + 2\frac{\kappa^2}{z_R^2}\right) \quad (2)$$

Where $\kappa = \pi L_{n\sqrt{\omega_c/2\omega}}$, $z_R = k_0 w_0^2/2$ and w_0 is the beam waist radius. It is possible for back-tunnelling to occur between the slow and fast X-mode [14], limiting the efficiency of the coupling at very high density gradients. This is not a concern for these plasmas however as the density gradients are too shallow to allow this to happen.

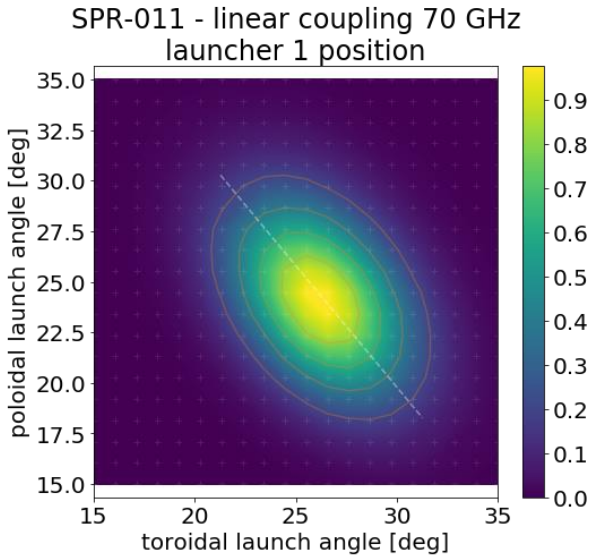

Fig. 7: An example of the coupling window for SPR-011 at 70 GHz, for a launching mirror placed 1 m from the plasma surface at the mid-plane. Calculations are for a single ray.

The EBW plasma scenario is still under development, but we present here some example calculations of SPR-011 at 70 GHz, which is the lowest frequency considered for this scenario and is likely a best case for EBW coupling. Fig. 7 shows a coupling window for a hypothetical launcher placed 1 m away from the plasma surface at the plasma midplane. There is a $\pm 1^o$ tolerance for 95% coupling, which is well inside present launcher capabilities. The density scale length, $L_n = n/\nabla n$, is estimated from a density profile which is calculated by EUROPED [15] to be consistent with the peeling ballooning stability limit for this plasma. Fig. 8, shows the coupling efficiency as a function of the increasing beam waist (decreasing divergence) at 70 GHz. We consider the density scale length uncertain at this stage, so we also show the performance for ½ and 2 times the nominal gradient estimated from EUROPED. We can see for this scenario that a 15 cm beam is sufficient to keep the coupling above 99% and larger beams mitigate the uncertainty in L_n to some degree.

In reality, this calculation misses the plasma curvature effects and the variation of the polarisation across the beam. These effects will limit the maximum conversion efficiency and will likely cause the curves in Fig. 8 to roll over. In order to estimate this effect, as well as the effects of density perturbations, we plan on performing 3D full wave simulations.

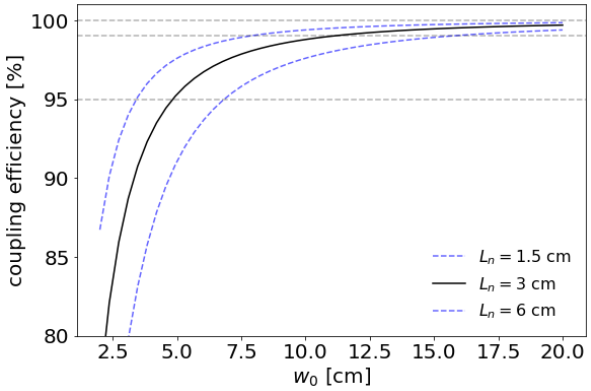

Fig. 8: The transmission coefficient as a function of the beam waist size. Larger beams have lower divergence and thus more efficient coupling.

4 EBCD system on MAST Upgrade

There are many physics challenges to be addressed before EBCD can become the default choice for current drive for STEP. Although there has been experimental evidence of efficient EBCD of $\zeta_{CD} \simeq 0.4$ on the stellarator [11], a more extensive validation of the current drive models for EBWs on STs is required. Furthermore, there has never been an experimental validation for the predictions of highly efficient current drive on STs of $\zeta_{CD} > 1$ [13], [16], which are also seen in our calculations for STEP. It has been shown that high-efficiency coupling from the LFS to EBW can be achieved [17], [18], but the effect of density perturbations and non-linear effects require more extensive investigation.

To provide an experimental basis for the use of EBCD on the spherical tokamak, an EBCD system will be installed on MAST Upgrade. The system consists of two dual-frequency gyrotrons (28/34.8 GHz), each capable of 900kW for 3 seconds or 800kW for 4.5 seconds. The aim of this system is to: provide an experimental test of the EBCD efficiency on an ST, examine open issues regarding the LFS coupling scheme, (such as the linear coupling behaviour and turbulence [19]), examine collisional damping and non-linear effects [20] and extend the original MAST experiments into EBW based solenoid-free start-up. An engineering design of the system can also be found at this workshop [21].

4.1 Coupling efficiency

In order to operate an EBW system on a modern experimental tokamak, it is necessary to show that the

power can be efficiently coupled to the plasma and that the stray radiation can be kept to a reasonable minimum.

In order to calculate the coupling efficiency for MAST Upgrade, we need to account for the possibility that the slow X-mode, which would normally convert 100% to the EBW, instead tunnels out of the plasma to the fast X-mode branch. This is different to STEP as the MAST Upgrade scale lengths are smaller and the frequency is lower. The efficiency of this process is given by [14], [22]:

$$\tau_{XX} = e^{-\pi\eta} \tag{3}$$

$$\eta = \left(1 - N_{\parallel}^2\right)^{3/2} \left[\frac{\omega_c L_n}{c\alpha}\left(\sqrt{(1+\alpha^2)} - 1\right)^{1/2}\right]_{UHR} \tag{4}$$

where $\alpha = \omega_p/\omega_c$, and the term in the square brackets is evaluated at the upper hybrid resonance. We also note the use of a square root for the α term in curved brackets, rather than the square found in [22]. The total reflectivity is then given by

$$R_{tot} = 1 - R_{XX} < \tau_{OX} >, \tag{5}$$

where $R_{XX} = 1 - \tau_{XX}$.

For this study, three separate full wave codes were employed, FFW, IPF-FDMC and EMIT-2D [19]. Initially, calculations were done in the plasma slab at 28 GHz. For the slab, $k_0 L_n = 25$, f = 28GHz, B_0 = 0.85 T and is directed parallel to the density contours.

As a numerical check of equation (2), the beam waist size was scanned and the coupling efficiency calculated with IPF-FDMC, the results of which are shown in Fig. 9. As can be seen from the Figure, the reflectivity from the full wave simulations is lower than predicted by the analytical result and it is suspected that this is due to the 2D nature of the full-wave simulations. This result however confirms the design choice to minimise the divergence of the launched O-mode. A scan of the phase front curvature at fixed divergence was also carried out, by altering the position of the beam focus, but only a negligible effect was seen in the coupling efficiency.

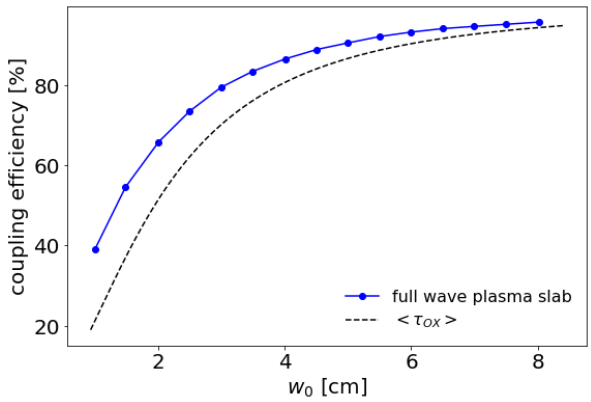

Fig. 9: The coupling efficiency vs beam waist size. The approximate formula in Equation (1) is plotted for comparison

To guide the frequency selection, we then scanned L_n and calculated the coupling efficiency. Fig. 10 shows the reflectivity from the full wave simulations, $1 - \tau_{OX}$, for this scan in blue. The green solid line is the reflectivity from Equation 2, the red dashed line indicates the transmission coefficient for the X-mode tunnelling, given in Equation 3 and the solid line indicates R_{tot}. It can be seen from the figure that there is a minimum in reflectivity for $k_0 L_n \simeq 5$, as the tunnelling from the slow to fast X-mode begins to dominate the reflectivity, and this corresponds well with the analytical estimate shown. We see good agreement between the analytical and full wave calculations on the position of the minimum, however the full wave simulations underestimate the reflectivity at higher $k_0 L_n$ due to their 2D nature. 3D full wave simulations are in progress to check if the analytical results presented here.

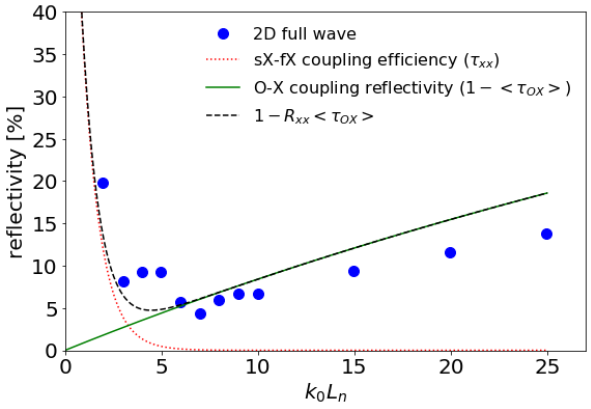

Fig. 10: The reflectivity as a function of density scale length. For small L_n, the reflectivity increases due to back-tunnelling of the slow X-mode to the fast X-mode

As realistic edge density gradients were not available for MAST Upgrade at the time the analysis was performed, example MAST shots were used. Fig. 11 left shows three example density profiles for H-mode, and low and high-density L-modes. The three dashed lines represent the cut-off densities for a fundamental harmonic (17.25 GHz), a second harmonic (35 GHz) and an intermediate frequency (28 GHz). As you can see from the figure, the fundamental harmonic causes a mode conversion at the bottom of the steep gradient region, and it is ambiguous as to whether this conversion would take place in the scrape off layer. Aside from an unpredictable gradient, the role of density perturbations in this region is likely much greater than for higher frequencies. Thus, it is preferred to have a second harmonic system.

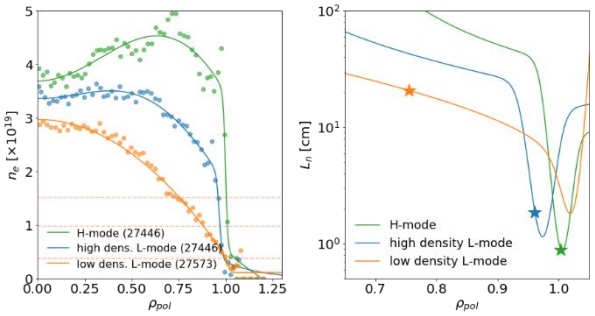

Fig. 11: Left: density profiles for H-mode, high-density L-mode and low-density L-mode. Dashed lines indicate cut-off densities for 17.25, 28 and 34.8 GHz. Right: density scale lengths for these profiles. Stars represent scale lengths at 34.8 GHz in each case.

The right panel of Fig. 11 shows the gradient scale lengths for the example profiles and the stars denote the scale lengths for 34.8 GHz for the three examples. Fig. 12 shows a similar figure to Fig. 10, but for MAST parameters for 34.8 GHz, $w_0 = 5.5$ cm. One can see that the high-density L-mode and H-mode are either side of the minimum in reflectivity, where the low-density L-mode shows a reflectivity of around 25%. Fig. 12 also shows there is a potential that if the density gradient in H-mode is increased from the estimated value here, the reflectivity could potentially rise quickly.

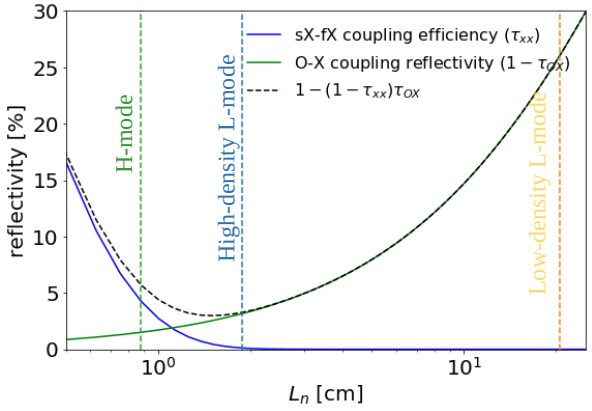

Fig. 12: The analytical reflectivity as a function of scale length for MAST Upgrade parameters. Dashed lines represent the expected scale lengths at the cut-off position for 34.8 GHz in H-mode, high-density, and low-density L-modes.

To catch the reflected beams, the system is designed with "interceptor plates". These are graphite plates placed in the path of the reflected beams and will be designed to scatter the reflected beam over a wide angular range, thus reducing the power density of any stray radiation in the vessel. Fig. 13 shows the approximate positions of these plates for the midplane launchers (similar plates are designed for the upper launchers) and the incident and reflected beams are shown at the optimal coupling angle for a plasma current of 800kA and 2000kA. The plates are also designed to work over the full range of plasma radii anticipated. The plates will be monitored with infrared cameras to measure the heating and this will be the primary diagnostic of reflected power (and thus coupling efficiency) for both machine protection and scientific purposes.

4.2 Current drive efficiency

In order to set the power requirements for the system, a critical factor was that a robustly measurable current could be driven. Initially the target was to be able to drive 10% of the plasma current and this was later supported with integrated modelling and forward modelling of the Motional Stark Effect diagnostic to find the ultimate sensitivity limitations. GENRAY and CQL3D were again used to predict the current drive efficiency. These predictions were performed before MAST Upgrade first plasma, so TRANSP [23] predictive design points were used. Fig. 14 shows the density and temperature profiles as well as the characteristic frequencies at the plasma midplane.

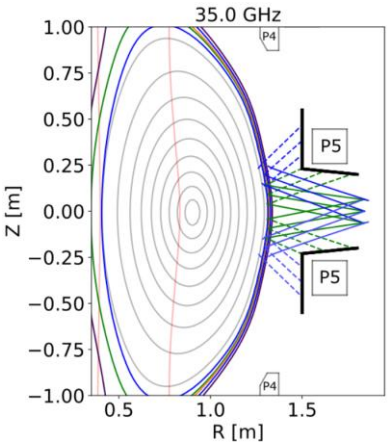

Fig. 13: A schematic plot of the poloidal cross-section of the beams from the midplane launcher for I_p = 800kA (green) and I_p = 2000 kA (blue). The dashed lines represent the beam reflected from the plasma after coupling. Thick black lines represent "interceptor plates".

A second harmonic system was preferred as the coupling is far more reliable at these frequencies, as shown in Section 4.1. From a launcher positioned on the machine midplane, it is possible to take advantage of a symmetry to drive co-current and counter-current at the same radial location, by coupling power into either the upper or lower coupling window. With two independent midplane launchers, one can drive any combination of co-current, counter-current, or balanced current (heating), greatly increasing the experimental flexibility of the system to disentangle heating and current drive effects. Furthermore, to drive current far off-axis without changing the gyrotron frequency, a pair of launchers are placed above the midplane (70 cm). For a detailed presentation of the launcher design please see [21].

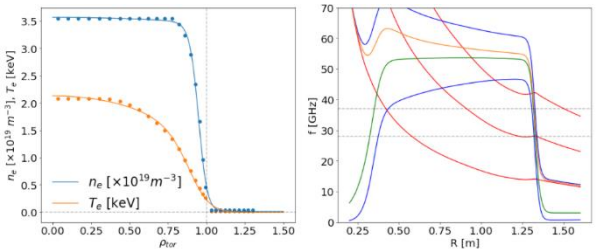

Fig. 14: Left: density and temperature profiles for MAST Upgrade TRANSP prediction C1a. Right: the characteristic frequencies of this scenario.

Current drive efficiencies between 0.1 A/W ($\zeta = 0.43$) and 0.14 A/W ($\zeta = 0.6$), shown in Fig. 15, were found close to the plasma axis, with the difference only being the plasma radius. EBW closer to the plasma centre appeared to gain a boost in CD efficiency. Since the plasma current in these scenarios is 1.2 MA, the requirement is then to have at least 1.2 MW of power coupled into the plasma as EBW.

5 Solenoid free start-up

It was shown on MAST that EBW, launched from the high field side, could provide highly efficient solenoid-free plasma start-up [5], [24]. This is of great interest to

the STEP programme as the solenoid in the STEP concepts is very limited in size and can only produce around 1MA at the plasma start-up. Any assistance that the heating system can provide would greatly assist the start-up phase. The MAST Upgrade experiments plan to increase both the power and time of the microwave radiation by up to a factor of ten, to further explore this novel technique. Similar calculations were performed for the off-midplane launcher, finding lower normalised efficiency of $\zeta = 0.3$, shown in Fig. 16.

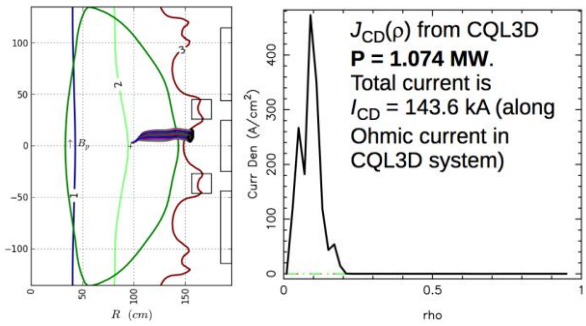

Fig. 15: Left: O-mode and EBW rays at 37 GHz. Right: the current density as calculated by CQL3D. The efficiency is 0.14 A/W and the corresponding ζ is 0.63

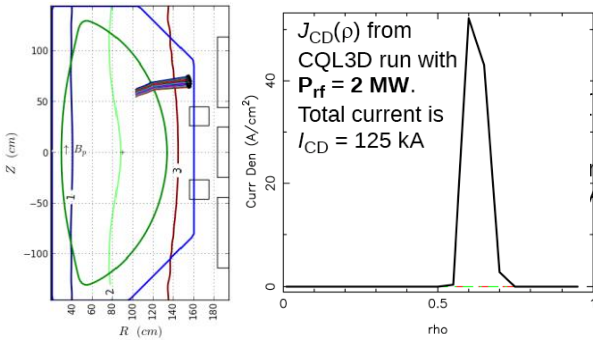

Fig. 16: off axis efficiency from a 70 cm high launcher. The efficiency is 0.063 A/W and the corresponding ζ is 0.3

6 Summary

In summary, the STEP spherical tokamak reactor will use microwave techniques for all heating and current drive requirements. ECCD is anticipated to be the primary source of auxiliary current drive due to its maturity and flexibility. However, EBCD is a planned opportunity due to its promise of high current drive efficiency at high density. GRAY was used to optimise the launch configuration for SPR scenarios finding efficiencies comparable to similar optimisations for ITER and EU-DEMO. EBCD was analysed using GENRAY and CQL3D and current drive efficiencies of around 3 times higher than ECCD were found, but this is limited to off-axis current drive as the penetration is limited by Doppler broadening and relativistic effects. The coupling to EBW was analysed using known analytical expressions, and the coupling was found to require large diameter beams to maintain high efficiency. The role of non-linearities and density perturbations remains to be investigated.

To provide a firm experimental basis for the use of EBCD, and solenoid free start-up for STEP, a 1.8 MW EBCD system will be installed on MAST Upgrade. The system is designed to give co-, counter- and balanced current from the midplane launcher, and could achieve greater than 10% of the total plasma current based on efficiency estimates using GENRAY/CQL3D. A launcher above the midplane will give off-axis deposition at the same frequency and magnetic field. A high coupling efficiency is expected, >96%, and interceptor plates are placed in the path of the reflected beam to decrease the power density of the stray radiation and serve as a measure of the coupling efficiency.

References

[1] D. Farina, “A Quasi-Optical Beam-Tracing Code for Electron Cyclotron Absorption and Current Drive: GRAY,” *Fusion Sci. Technol.*, vol. 52, no. 2, pp. 154–160, Aug. 2007.

[2] L. Figini, “Electron Cyclotron Current Drive Efficiency in the STEP Device,” *EPJ Web Conf.*, p. under review, 2022.

[3] T. C. Luce *et al.*, “Generation of Localized Noninductive Current by Electron Cyclotron Waves on the DIII-D Tokamak,” *Phys. Rev. Lett.*, vol. 83, no. 22, pp. 4550–4553, Nov. 1999.

[4] E. Poli *et al.*, “Electron-cyclotron-current-drive efficiency in DEMO plasmas,” *Nucl. Fusion*, vol. 53, no. 1, p. 013011, Jan. 2013.

[5] V. Shevchenko, Y. Baranov, M. O’Brien, and A. Saveliev, “Generation of Noninductive Current by Electron-Bernstein Waves on the COMPASS-D Tokamak,” *Phys. Rev. Lett.*, vol. 89, no. 26, p. 265005, Dec. 2002.

[6] A. P. Smirnov and R. W. Harvey, “The GENRAY Ray Tracing Code,” 2003. [Online]. Available: https://www.compxco.com/Genray_manual.pdf . [Accessed: 01-Jul-2022].

[7] R. . Harvey and M. . McCoy, “The CQL3D Fokker-Planck Code,” 2015. [Online]. Available: https://www.compxco.com/cql3d_manual.pdf. [Accessed: 01-Jul-2022].

[8] T. Wilson, “Electron Bernstein Wave (EBW) current drive profiles and efficiency for STEP,” *EPJ Web Conf.*, p. under review, 2022.

[9] J. Preinhaelter and V. Kopecký, “Penetration of high-frequency waves into a weakly inhomogeneous magnetized plasma at oblique incidence and their transformation to Bernstein modes,” *J. Plasma Phys.*, vol. 10, no. 1, pp. 1–12, Aug. 1973.

[10] A. Mueck *et al.*, “Demonstration of Electron-Bernstein-Wave Heating in a Tokamak via O−X−B Double-Mode Conversion,” *Phys. Rev. Lett.*, vol. 98, no. 17, p. 175004, Apr. 2007.

[11] H. P. Laqua, H. Maassberg, N. B. Marushchenko, F. Volpe, A. Weller, and W. Kasparek, “Electron-Bernstein-Wave Current Drive in an Overdense Plasma at the

Wendelstein 7-AS Stellarator," *Phys. Rev. Lett.*, vol. 90, no. 7, p. 075003, Feb. 2003.
[12] E. Mjølhus, "Coupling to Z mode near critical angle," *J. Plasma Phys.*, vol. 31, no. 1, pp. 7–28, Feb. 1984.
[13] J. Urban *et al.*, "A survey of electron Bernstein wave heating and current drive potential for spherical tokamaks," *Nucl. Fusion*, vol. 51, no. 8, p. 083050, Aug. 2011.
[14] A. K. Ram and S. D. Schultz, "Excitation, propagation, and damping of electron Bernstein waves in tokamaks," *Phys. Plasmas*, vol. 7, no. 10, p. 4084, 2000.
[15] S. Saarelma *et al.*, "Self-consistent pedestal prediction for JET-ILW in preparation of the DT campaign," *Phys. Plasmas*, vol. 26, no. 7, p. 072501, Jul. 2019.
[16] G. Taylor *et al.*, "Efficient generation of noninductive, off-axis, Ohkawa current, driven by electron Bernstein waves in high β, spherical torus plasmas," *Phys. Plasmas*, vol. 11, no. 10, pp. 4733–4739, Oct. 2004.
[17] G. Taylor *et al.*, "Efficient coupling of thermal electron Bernstein waves to the ordinary electromagnetic mode on the National Spherical Torus Experiment," *Phys. Plasmas*, vol. 12, no. 5, p. 052511, May 2005.
[18] H. P. Laqua, V. Erckmann, H. J. Hartfuß, and H. Laqua, "Resonant and Nonresonant Electron Cyclotron Heating at Densities above the Plasma Cutoff by O-X-B Mode Conversion at the W7-As Stellarator," *Phys. Rev. Lett.*, vol. 78, no. 18, pp. 3467–3470, May 1997.
[19] A. Koehn-Seemann, "Numerical investigations of the O-X mode conversion process in MAST Upgrade," *EPJ Web Conf.*, p. under review, 2022.
[20] M. Senstius, "Nonlinear degradation of O-X-B in MAST Upgrade," *EPJ Web Conf.*, p. under review, 2022.
[21] H. Webster, "MAST Upgrade Microwave Heating and Current Drive System - Engineering Design Overview," *EPJ Web Conf.*, p. under review, 2022.
[22] A. . Ram and A. Bers, "Excitation and emission of electron cyclotron waves in spherical tori," *Nucl. Fusion*, vol. 43, no. 11, pp. 1305–1312, Nov. 2003.
[23] "TRANSP users pages." [Online]. Available: https://transp.pppl.gov/index.html.
[24] V. F. Shevchenko *et al.*, "Long Pulse EBW Start-up Experiments in MAST," *EPJ Web Conf.*, vol. 87, p. 02007, Mar. 2015.